THE JOURNAL OF BIOLOGICAL CHEMISTRY VOL. 284, NO. 50, pp. 34648–34657, December 11, 2009

Low Micromolar Zinc Accelerates the Fibrillization of Human Tau via Bridging of Cys-291 and Cys-322*

Received for publication, August 24, 2009 Published, JBC Papers in Press, October 13, 2009, DOI 10.1074/jbc.M109.058883

Zhong-Ying Mo, Ying-Zhu Zhu, Hai-Li Zhu, Jun-Bao Fan, Jie Chen, and Yi Liang[1]

From the State Key Laboratory of Virology, College of Life Sciences, Wuhan University, Wuhan 430072, China

A hallmark of a group of neurodegenerative diseases such as Alzheimer disease is the formation of neurofibrillary tangles, which are principally composed of bundles of filaments formed by microtubule-associated protein Tau. Clarifying how natively unstructured Tau protein forms abnormal aggregates is of central importance for elucidating the etiology of these diseases. There is considerable evidence showing that zinc, as an essential element that is highly concentrated in brain, is linked to the development or progression of these diseases. Herein, by using recombinant human Tau fragment $Tau_{244-372}$ and its mutants, we have investigated the effect of zinc on the aggregation of Tau. Low micromolar concentrations of Zn^{2+} dramatically accelerate fibril formation of wild-type $Tau_{244-372}$ under reducing conditions, compared with no Zn^{2+}. Higher concentrations of Zn^{2+}, however, induce wild-type $Tau_{244-372}$ to form granular aggregates in reducing conditions. Moreover, these non-fibrillar aggregates assemble into mature Tau filaments when Zn^{2+} has been chelated by EDTA. Unlike wild-type $Tau_{244-372}$, low micromolar concentrations of Zn^{2+} have no obvious effects on fibrillization kinetics of single mutants C291A and C322A and double mutant C291A/C322A under reducing conditions. The results from isothermal titration calorimetry show that one Zn^{2+} binds to one Tau molecule via tetrahedral coordination to Cys-291 and Cys-322 as well as two histidines, with moderate, micromolar affinity. Our data demonstrate that low micromolar zinc accelerates the fibrillization of human Tau protein via bridging Cys-291 and Cys-322 in physiological reducing conditions, providing clues to understanding the relationship between zinc dyshomeostasis and the etiology of neurodegenerative diseases.

Tau, a microtubule-associated protein, is the major protein subunit of neurofibrillary tangles (NFTs),[2] which are found in a group of neurodegenerative diseases such as Alzheimer disease and frontotemporal lobar degeneration (1, 2). NFTs are mainly composed of bundles of Tau in the form of paired helical filaments (PHFs), straight filaments, or twisted ribbons. It is generally believed that the neuron degeneration in such diseases is very likely to be contributed by the accumulation of these aggregates (3). Thus the characterization of factors involved in abnormal Tau aggregation is of great importance to clarify the etiology of neurodegenerative diseases and assist in the establishment of medical treatment.

Tau is one of the largest proteins without recognizable secondary structure and adopts a natively unfolded structure in solution (4). There are two distinct domains of Tau protein, the projection domain and the microtubule binding domain. The microtubule binding domain mainly contains either three or four imperfect repeats (18 amino acids in length) separated from one another by inter repeats (13–14 amino acids in length) (5). In its normal state, Tau facilitates and stabilizes the assembly of microtubules. But under certain pathological conditions, it will detach from microtubules. Some of its small segments adopt a β-conformation, and further interactions convert them toward formation of aggregates that are rich in β-sheet structures. These aggregates undergo filament nucleation and elongation and form NFTs eventually (1, 2, 6). The microtubule binding repeat region forms the core of filaments while the rest of the protein retains its largely unfolded structure, which forms the fuzzy coat of the filaments (7–9).

Although the mechanism by which Tau protein aggregates is not fully understood, there are increasing evidences showing that a disturbance of brain zinc homeostasis during aging plays a role in the etiology of Alzheimer disease (10–12). Zinc is an integral component of numerous enzymes, transcription factors, and structural proteins. Furthermore, zinc is one of the most abundant transition metals in the brain and is in particularly large concentrations in the mammalian brain with an overall concentration of ~150 μM (13). The distribution of zinc is not uniform, and up to 15% of brain zinc is located inside presynaptic vesicles (13, 14). Although the cytosolic free concentration of Zn^{2+} in cultured neurons is generally subnanomolar, in pathological conditions the free concentration of Zn^{2+} is altered via several pathways such as presynaptic zinc translocation (15).

There is current evidence for a relative increase in intracellular zinc in vulnerable regions of the Alzheimer disease brain (16), and abnormally high levels of zinc at millimolar concentrations have been found in NFTs and senile plaque cores (17, 18). It is estimated that strong activation of Zn^{2+}-containing presynaptic terminals results in transient local synaptic Zn^{2+} concentrations in the 100–300 μM range (13, 17). Histochemically reactive zinc deposits are also found specifically localized to cerebral amyloid angiopathy deposits and NFT-bearing neurons (19). It has been reported that there are 3- to 5-fold increases in zinc in the cortical and accessory basal nuclei of the

* This work was supported by National Key Basic Research Foundation of China Grant 2006CB910301 and by National Natural Science Foundation of China Grants 30770421 and 30970599.

[1] To whom correspondence should be addressed. Tel.: 86-27-6875-4902; Fax: 86-27-6875-4902; E-mail: liangyi@whu.edu.cn.

[2] The abbreviations used are: NFT, neurofibrillary tangles; AFM, atomic force microscopy; DM, double mutant C291A/C322A of $Tau_{244-372}$; DTT, dithiothreitol; ITC, isothermal titration calorimetry; PHF, paired helical filaments; TEM, transmission electron microscopy; ThT, thioflavin T; WT, wild-type $Tau_{244-372}$.

amygdala and in the neuropil of Alzheimer disease patients, as compared with age-matched controls (20).

Zinc has been shown to accelerate the aggregation of amyloid β peptides (21, 22), trigger the fibrillization of methionine oxidized α-synuclein (23), and cause an aggregation of Dcp1a protein in an RNA-dependent manner (24). There are also results indicating that Ca^{2+} and Mg^{2+} can selectively induce the formation of PHF-Tau aggregation (25), whereas Al^{3+}, Cu^{2+}, and Fe^{2+}/Fe^{3+} can bind to Tau (26–28). However, whether Zn^{2+} has an effect on the aggregation of Tau has not been reported so far, which leaves us to answer the physiological question whether the alteration of zinc can affect Tau aggregation and thus play a role in the pathology of neurodegenerative diseases such as Alzheimer disease.

In the present study, by using several biophysical methods, such as thioflavin T binding, atomic force microscopy (AFM), transmission electron microscopy (TEM), and isothermal titration calorimetry (ITC), we investigated the impact of zinc on the aggregation of human Tau fragment $Tau_{244-372}$. Our results indicated that low micromolar zinc dramatically accelerated fibril formation of wild-type $Tau_{244-372}$ in the presence of dithiothreitol (DTT), but had no obvious effects on fibrillization kinetics of single mutants C291A and C322A and double mutant C291A/C322A. Further, we demonstrated that Zn^{2+} bound to Tau molecules via tetrahedral coordination to Cys-291, Cys-322, and two histidines with moderate, micromolar affinity, and thus concluded that low micromolar zinc promoted the fibrillization of human Tau protein via bridging of Cys-291 and Cys-322 in physiological reducing conditions.

EXPERIMENTAL PROCEDURES

Materials—Heparin (average molecular mass = 6 kDa) and thioflavin T (ThT) were purchased from Sigma. DTT was obtained from Ameresco Chemical Co. (Solon, OH). All the metal cations used were chloride forms of analytical grade. All other chemicals used were made in China and were of analytical grade. The buffers used in this study were treated with ion-exchange resins to remove trace amounts of divalent cations present as contaminants in the solutions.

Plasmids and Proteins—The cDNA-encoding human Tau fragment $Tau_{244-372}$ was amplified using the plasmid for human Tau40 (kindly provided by Dr. Michel Goedert) as a template. The PCR-amplified $Tau_{244-372}$ was subcloned into pRK172 vector. Single cysteine mutants C291A and C322A and double mutant C291A/C322A of $Tau_{244-372}$ were generated using primers GCAACGTCCAGTCCAAGGCTGGCTCAAAGG/CCTTTGAGCCAGCCTTGGACTGGACGTTGC for C291A and GTGACCTCCAAGGCTGGCTCATTAGGCAACATC/GATGTTGCCTAATGAGCCAGCCTTGGAGGTCAC for C322A. Single histidine mutants H330A and H362A and histidine-less mutant H268A/H299A/H329A/H330A/H362A were generated in a similar manner. Plasmids containing target sequences were transformed into *Escherichia coli* BL21 (DE3) strain. The expression of recombinant human Tau fragment $Tau_{244-372}$ and its mutants was induced with 400 μM isopropyl-β-D-thiogalactopyranoside and cultured for 3 h. Cell pellets of 2-liter culture were collected and re-suspended in 80 ml of buffer A (20 mM phosphate buffer containing 2 mM DTT, pH 7.0) and then sonicated at 250 watts for 30 min. 500 mM NaCl was added into the mixture, and then the mixture was boiled at 100 °C for 15 min. After centrifugation at 17,000 × *g* for 30 min at 4 °C, supernatant was collected and dialyzed against buffer A extensively. The sample was then loaded to an SP-Sepharose column and washed with 400 ml of buffer A. The target protein was obtained by washing the column using 500 ml of 20 mM phosphate buffer containing 2 mM DTT and 0–400 mM NaCl. The Tau fragment was then concentrated and dialyzed against 50 mM Tris-HCl buffer containing 2 mM DTT (pH 7.5) extensively, and then stored at −80 °C. Purified Tau protein was analyzed by SDS-PAGE with one band and confirmed by mass spectrometry. The concentration of human Tau fragment was determined according to its absorbance at 214 nm with a standard calibration curve drawn by bovine serum albumin as described (29).

ThT Binding Assays—A 2.5 mM ThT stock solution was freshly prepared in 50 mM Tris-HCl buffer (pH 7.5) and passed through a 0.22-μm pore size filter before use to remove insoluble particles. Under standard conditions, 10 μM $Tau_{244-372}$ was incubated without agitation in 50 mM Tris-HCl buffer (pH 7.5) containing 1 mM DTT and 20 μM ThT with or without Zn^{2+} at 37 °C for up to 1 h in the presence of fibrillization inducer heparin used in a Tau:heparin molar ratio of 4:1. The fluorescence of ThT was excited at 440 nm with a slit width of 7.5 nm, and the emission was measured at 480 nm with a slit width of 7.5 nm on an LS-55 luminescence spectrometer (PerkinElmer Life Sciences). The preparation of the samples before the first measurement took 1 min.

The polymerization for $Tau_{244-372}$ and its cysteine mutants in 96-well plates were set up by a mixture of 20 μM Tau protein, 5 μM heparin, 50 μM ThT, and 0–80 μM Zn^{2+} either in the presence or in the absence of 1 mM DTT in 50 mM Tris-HCl buffer containing 100 mM NaCl (pH 7.5). The reaction components were mixed quickly and immediately read for 8 h (with DTT) or 3 h (without DTT) at 37 °C in SpectraMax M2 microplate reader (Molecular Devices, Sunnyvale, CA) using excitation at 440 nm and emission at 480 nm with a wavelength cut-off at 475 nm. Each sample was run in triplicate or quadruplicate. Kinetic parameters were determined by fitting ThT fluorescence intensity *versus* time to a sigmoidal equation (30),

$$F = F_0 + (A + ct)/\{1 + \exp[k(t_m - t)]\} \qquad \text{(Eq. 1)}$$

where F is the fluorescence intensity, k is the rate constant for the growth of fibrils, and t_m is the time to 50% of maximal fluorescence. The initial baseline during the lag time is described by F_0. The final baseline after the growth phase has ended is described by $A + ct$. The lag time is calculated as $t_m - 2/k$.

Sarkosyl-insoluble Tau SDS-PAGE—The Sarkosyl-insoluble Tau experiments were carried out according to the method described by Aoyagi and co-workers (31) with minor changes. Tau polymerization was set up by incubating a mixture of 10 μM $Tau_{244-372}$, 2.5 μM heparin, 1 mM DTT, and 0–100 μM Zn^{2+} in 50 mM Tris-HCl buffer (pH 7.5) at 37 °C without agitation. Aliquots (100 μl) of assembly mixtures were taken out and added

into 500 μl of 50 mM Tris-HCl buffer (pH 7.5) containing 1% Sarkosyl. The mixture was left at room temperature for 30 min and then centrifuged in an Optima LE-80K ultracentrifuge (Beckman Coulter, Fullerton, CA) at 150,000 × *g* for 30 min. The supernatant (Sarkosyl-soluble Tau) was removed, and the pellet (Sarkosyl-insoluble Tau) was re-suspended in 50 μl of SDS sample buffer containing 5% 2-mercaptoethanol and subjected to 15% SDS-PAGE. After the electrophoresis the gels were stained with Coomassie Blue.

Transmission Electron Microscopy—The formation of filaments by human Tau fragment was confirmed by electron microscopy of negatively stained samples. Sample aliquots of 10 μl were placed on copper grids and left at room temperature for 1–2 min, rinsed with H_2O twice, and then stained with 2% (w/v) uranyl acetate for another 1–2 min. The stained samples were examined using an H-8100 transmission electron microscope (Hitachi, Tokyo, Japan) operating at 100 kV.

AFM—The formation of filaments by human Tau fragment was further confirmed by AFM. Sample aliquots of 10 μl were deposited onto freshly cleaved mica, left on the surface for 10 min, and rinsed with H_2O twice. Then the solution was dried in a desiccator for 12 h. AFM images were acquired in tapping mode with an SPM-9500 J3 scanning probe microscope (Shimadzu, Kyoto, Japan). Several regions of the mica surface were examined to confirm that similar structures existed through the sample.

Isothermal Titration Calorimetry—ITC experiments on the interaction of Zn^{2+} with $Tau_{244-372}$ and its mutants were carried out at 25.0 °C using an iTC_{200} titration calorimetry (MicroCal, Northampton, MA). Freshly purified Tau proteins (wild-type $Tau_{244-372}$, single mutants C291A, C322A, H330A, and H362A, double mutant C291A/C322A, and histidine-less mutant H268A/H299A/H329A/H330A/H362A) were dialyzed against 50 mM Tris-HCl buffer (pH 7.5) containing 1 mM EDTA, overnight at 4 °C and then dialyzed against 50 mM Tris-HCl buffer (pH 7.5) extensively to remove EDTA. A solution of 100–200 μM Tau proteins was loaded into the sample cell (200 μl), and a solution of 2.8–6.0 mM Zn^{2+} was placed in the injection syringe (40 μl). The first injection (0.3 μl) was followed by 24–27 injections of 1 μl. Dilution heats of Zn^{2+} were measured by injecting Zn^{2+} solution into buffer alone and were subtracted from the experimental curves prior to data analysis. The stirring rate was 600 rpm. The resulting data were fitted to a single set of identical sites model using MicroCal ORIGIN software supplied with the instrument, and the standard molar enthalpy change for the binding, $\Delta_b H^0_m$, the dissociation constant, K_d, and the binding stoichiometry, n, were thus obtained. The standard molar free energy change, $\Delta_b G^0_m$, and the standard molar entropy change, $\Delta_b S^0_m$, for the binding reaction were calculated by the fundamental equations of thermodynamics (32).

$$\Delta_b G^0_m = RT \ln K_d \quad \text{(Eq. 2)}$$

$$\Delta_b S^0_m = (\Delta_b H^0_m - \Delta_b G^0_m)/T \quad \text{(Eq. 3)}$$

RESULTS

The Presence of Zn^{2+} Influenced Tau Aggregation—The enhanced fluorescence emission of the dye ThT has been frequently used for monitoring the kinetics of amyloid fibril formation, which is a specific marker for the β-sheet conformation of fibril structures (33, 34). Because $Tau_{244-372}$ consists of the four-repeat microtubule binding domain forming the core of PHFs in Alzheimer disease and assembles more readily than full-length Tau protein into filaments in *vitro*, we employed such a Tau fragment for studying kinetics of Tau fibril formation. As shown in Fig. 1, the kinetic curves of the ThT fluorescence intensity at 480 nm for $Tau_{244-372}$ fibrillization were consistent with a nucleation-dependent elongation model (35), in which the lag phase corresponded to the nucleation phase, and the exponential part to a fibril growth (elongation) phase.

Bivalent cations such as Mg^{2+}, Mn^{2+}, Ca^{2+}, Zn^{2+}, and Cu^{2+} and trivalent cation Fe^{3+} were incubated separately with physiological concentrations of $Tau_{244-372}$ at 37 °C in the presence of DTT. As shown in Fig. 1*A*, in the absence of cation, the lag phase for wild-type $Tau_{244-372}$ polymerization was ~500 s, whereas the addition of Mg^{2+}, Mn^{2+}, Ca^{2+}, Fe^{3+}, and Cu^{2+} at a low micromolar concentration (10 μM) decreased the lag phase in different ranges. In the presence of 10 μM Zn^{2+}, however, the lag phase was dramatically diminished, indicating that low micromolar concentrations of Zn^{2+} greatly accelerated fibril formation of wild-type $Tau_{244-372}$, compared with no Zn^{2+}, and the enhancing effect of Zn^{2+} was more remarkable than those of other cations such as Mn^{2+}, Fe^{3+}, and Cu^{2+}. Clearly, the nucleation of Tau fragment was much more accelerated by 10 μM Zn^{2+} than the following step of elongation (Fig. 1*A*). Meanwhile, when wild-type $Tau_{244-372}$ was incubated with 100 μM cations, the kinetic curve of $Tau_{244-372}$ in the presence of Zn^{2+} was also quite different from those of other cations except Fe^{3+} (Fig. 1*B*). The lag phase was too short to be observed, but the maximum intensity became much lower in the presence of 100 μM Zn^{2+} than that in the absence of cation, indicating the aggregation of $Tau_{244-372}$ was significantly altered by higher concentrations of Zn^{2+}. Both cases indicated that the presence of Zn^{2+}, compared with other cations, significantly altered the aggregation of Tau in reducing conditions and factors other than electrostatic interactions must play a role in this phenomenon.

To get a better understanding about the effect of zinc on Tau aggregation, we performed ThT binding assays at various concentrations of Zn^{2+}. As shown in Fig. 1*C*, the addition of 5–20 μM Zn^{2+} accelerated fibril formation of wild-type $Tau_{244-372}$ under reducing conditions, but the enhancing effect of Zn^{2+} was most significant when the concentration of Zn^{2+} was 10 μM, which is equal to that of Tau fragment. When the concentration of Zn^{2+} went higher, the kinetic curves still went up instantly, almost without a lag phase, but the final ThT intensities decreased 65 and 76% for 50 and 100 μM Zn^{2+}, respectively (Fig. 1*C*). The phenomenon that the presence of Zn^{2+} significantly reduced the lag phase indicated that Zn^{2+} had a strong enhancing effect on the nucleation of Tau protein. However, smaller exponential growth at higher molar ratios of Zn^{2+} to Tau suggested fewer filaments but other forms of Tau aggregates were formed, compared with no Zn^{2+}.

To semi-quantify the aggregates of Tau protein formed in the presence of Zn^{2+} at different concentrations, we carried out Sarkosyl-insoluble SDS-PAGE experiments and assessed

$Tau_{244-372}$ aggregation under reducing conditions by measuring the Sarkosyl-insoluble Tau as described (31). As shown in Fig. 1*D*, a clear band corresponding to Sarkosyl-insoluble Tau filaments was observed when wild-type $Tau_{244-372}$ was incubated in the absence of Zn^{2+} for 40 min, whereas the Sarkosyl-insoluble Tau band was observed when $Tau_{244-372}$ was incubated with Zn^{2+} at low micromolar concentrations (5–10 μM) for a much shorter time (15–10 min). Furthermore, when $Tau_{244-372}$ was incubated for 40 min, the intensity of the Sarkosyl-insoluble Tau band in the presence of 10 μM Zn^{2+} was remarkably higher than that in the absence of Zn^{2+}. This finding further supports the observation mentioned above that low micromolar concentrations of Zn^{2+} dramatically accelerate fibril formation of wild-type $Tau_{244-372}$ in reducing conditions, compared with no Zn^{2+}. At higher concentrations of Zn^{2+} (50–100 μM), however, no Sarkosyl-insoluble Tau band was observed even at 40 min (Fig. 1*D*), indicating that fewer filaments but other forms of Tau aggregates, Sarkosyl-soluble Tau aggregates, were formed at higher molar ratios of Zn^{2+} to Tau under reducing conditions.

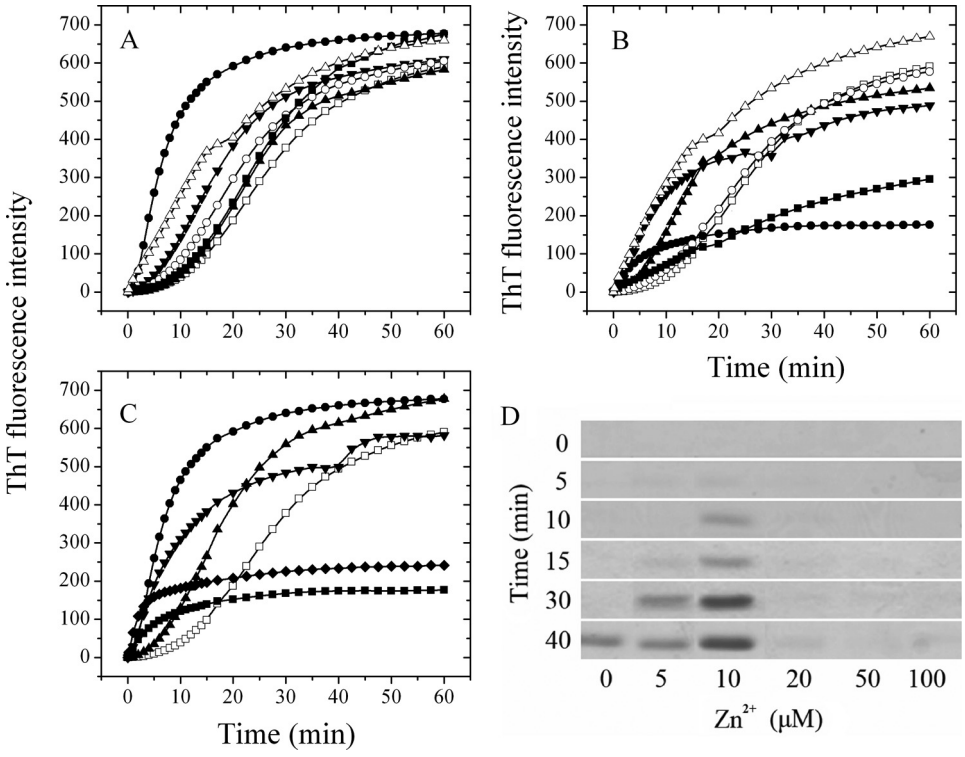

FIGURE 1. **The presence of Zn^{2+} altered $Tau_{244-372}$ fibrillization kinetics.** *A*, 10 μM $Tau_{244-372}$ was incubated with 10 μM cation (*open circle*, Mg^{2+}; *filled triangle*, Mn^{2+}; *filled inverted triangle*, Ca^{2+}; *filled circle*, Zn^{2+}; *filled square*, Fe^{3+}; and *open triangle*, Cu^{2+}) or without cation (*open square*); *B*, 10 μM $Tau_{244-372}$ was incubated with 100 μM cation (*open circle*, Mg^{2+}; *filled triangle*, Mn^{2+}; *filled inverted triangle*, Ca^{2+}; *filled circle*, Zn^{2+}; *filled square*, Fe^{3+}; and *open triangle*, Cu^{2+}) or without cation (*open square*); *C*, 10 μM $Tau_{244-372}$ was incubated with 0–100 μM Zn^{2+} (*open square*, 0 μM; *filled triangle*, 5 μM; *filled circle*, 10 μM; *filled inverted triangle*, 20 μM; *filled rhombus*, 50 μM; and *filled square*, 100 μM). The buffer used was 50 mM Tris-HCl buffer (pH 7.5) containing 1 mM DTT, 2.5 μM heparin, and 20 μM ThT, and ThT binding assays were carried out at 37 °C. *D*, 10 μM $Tau_{244-372}$ was incubated with 0–100 μM Zn^{2+} containing 2.5 μM heparin and 1 mM DTT in 50 mM Tris-HCl buffer (pH 7.5) at 37 °C. Aliquots were taken at 0, 5, 10, 15, 30, and 40 min, respectively, and then incubated with Tris-HCl buffer containing 1% Sarkosyl followed by centrifuging at 150,000 × *g* for 30 min. Pellets were re-suspended with sample buffer containing 5% 2-mercaptoethanol and subjected to 15% SDS-PAGE. Gels were stained with Coomassie Blue.

Morphology of Tau Aggregates Varied with Molar Ratios of Zn^{2+} to Tau—TEM and AFM were employed to study the morphology of wide-type $Tau_{244-372}$ incubated with Zn^{2+} at different concentrations for 60 min (Fig. 2). The addition of low micromolar concentrations of Zn^{2+} (5 or 10 μM) had no significant effect on the morphology of Tau samples monitored by TEM and AFM, and long and branched fibrils as well as a few short filaments (Fig. 2, *A–C*) and some filaments with a length of 200–500 nm (Fig. 2, *G–I*) were observed in these three samples. When the concentration of Zn^{2+} increased (50 or 100 μM) until the molar ratio of Zn^{2+} to Tau exceeded equality, however,

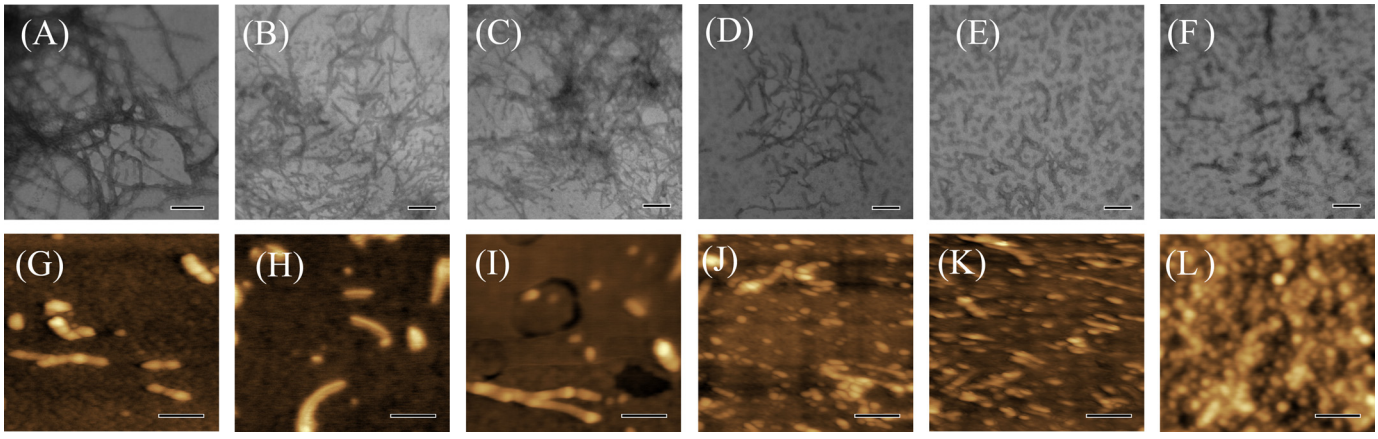

FIGURE 2. **Transmission electron micrographs (*A–F*) and AFM images (*G–L*) of $Tau_{244-372}$ aggregates formed with Zn^{2+}.** 10 μM $Tau_{244-372}$ was incubated with 0–100 μM Zn^{2+} (*A* and *G*, 0 μM; *B* and *H*, 5 μM; *C* and *I*, 10 μM; *D* and *J*, 20 μM; *E* and *K*, 50 μM; and *F* and *L*, 100 μM) containing 2.5 μM heparin and 1 mM DTT in 50 mM Tris-HCl buffer (pH 7.5) at 37 °C for 60 min. A 2% (w/v) uranyl acetate solution was used to negatively stain the fibrils (*A–F*). The *scale bars* represent 200 nm.

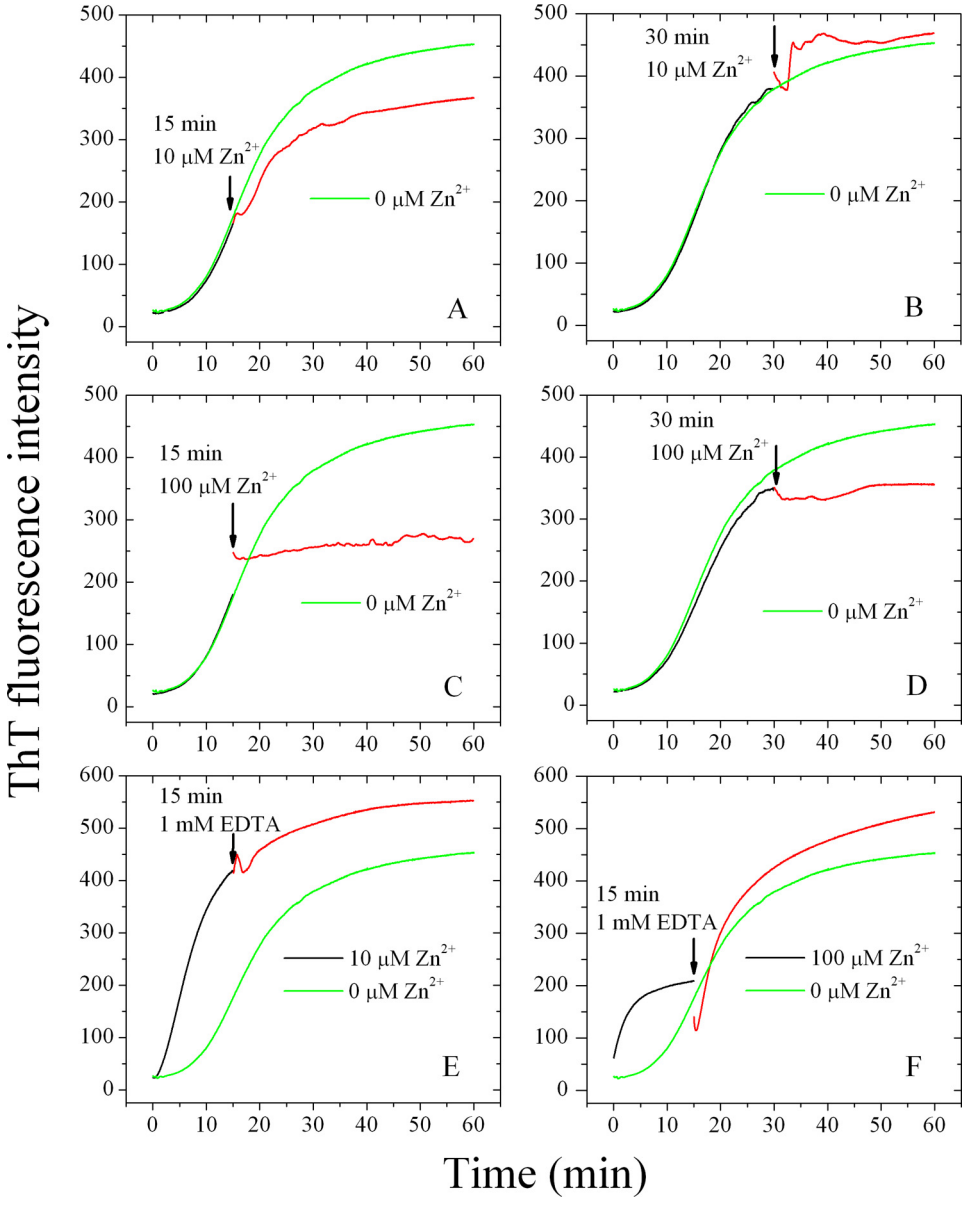

FIGURE 3. **Effect of Zn^{2+} on $Tau_{244-372}$ fibrillization at various time points.** 10 μM $Tau_{244-372}$ was incubated without Zn^{2+} (*black curves*) and then titrated with 10 μM Zn^{2+} or 100 μM Zn^{2+} at 15 min (*A* and *C*) or 30 min (*B* and *D*) respectively (*red curves*). *E*, 10 μM $Tau_{244-372}$ was incubated with 10 μM Zn^{2+} (*black curves*) and then titrated with aliquots of 1 mM EDTA at 15 min (*red curves*). *F*, 10 μM $Tau_{244-372}$ was incubated with 100 μM Zn^{2+} (*black curves*) and then titrated with 1 mM EDTA at 15 min (*red curves*). The beginning of titrations is indicated by *black arrows*, and the curves are compared with 10 μM $Tau_{244-372}$ incubated without Zn^{2+} (*green curves*). The buffer used was 50 mM Tris-HCl buffer (pH 7.5) containing 1 mM DTT, 2.5 μM heparin, and 20 μM ThT, and ThT binding assays were carried out at 37 °C.

$Tau_{244-372}$ filaments became much fewer and shorter, and abundant granular aggregates (~30 nm in diameter) were observed (Fig. 2, *E*, *F*, *K*, and *L*). Maeda and co-workers (36) have observed similar aggregates and have suggested that such granular Tau aggregates may be an intermediate form of Tau fibrils.

Combining the results from TEM and AFM, we concluded that the morphology of wild-type $Tau_{244-372}$ aggregates varied with molar ratios of Zn^{2+} to Tau in reducing conditions. At lower molar ratios, Tau aggregates were mainly composed of filaments, which was similar to those in the absence of Zn^{2+}. But at higher molar ratios, filaments became much fewer and shorter, and granular aggregates became prevalent. In other words, higher concentrations of Zn^{2+} induced wild-type $Tau_{244-372}$ to form granular aggregates under reducing conditions.

Characterization of the Effect of Zinc on Tau Aggregation at Different Stages—We then checked whether the enhancing effect of Zn^{2+} on the aggregation of Tau was dependent on the incubation time or different compositions of Tau protein. We added 10 or 100 μM Zn^{2+} after incubation for 5, 15, and 30 min, when $Tau_{244-372}$ was no longer pure monomers. As shown in Fig. 3 (*A–D*), Zn^{2+} added at 15 min in the growth phase or at 30 min in the final equilibrium phase did not facilitate fibril formation of $Tau_{244-372}$ under reducing conditions; on the contrary, it slowed down or even blocked the growth phase. Furthermore, 10 μM Zn^{2+} added at 5 min in the lag phase had no obvious effect on fibril formation of $Tau_{244-372}$, and 100 μM Zn^{2+} added at 5 min slowed down the growth phase in reducing conditions (data not shown). The above results suggested that the enhancing effect on fibrillization kinetics of Tau by low micromolar concentrations of Zn^{2+} was mainly due to its direct interaction with Tau monomers, but not protofibrils or fibrils. It is this interaction that accelerated the nucleation of Tau protein.

To verify whether the effect of Zn^{2+} was chelator-reversible, we added 1 mM EDTA into systems containing $Tau_{244-372}$ incubated with 10 or 100 μM Zn^{2+} separately. As shown in Fig. 3 (*E* and *F*), the addition of EDTA at 15 min in the growth phase did not change fibrillization kinetics of Tau in the presence of 10 μM Zn^{2+}, suggesting that, once the nucleation of Tau had been finished, the binding of Zn^{2+} to Tau was no longer necessary for the filament elongation and maturation. But in the presence of 100 μM Zn^{2+}, the addition of EDTA at 15 min did alter the fibrillization kinetics by accelerating the elongation of Tau protein remarkably and reaching a final ThT intensity ~17% larger than that in the absence of Zn^{2+}. Higher concentrations of Zn^{2+} induced Tau to form granular aggregates under reducing conditions (Fig. 2). Moreover, such non-fibrillar aggregates assembled into mature Tau filaments when Zn^{2+} had been chelated by EDTA (Fig. 3*F*).

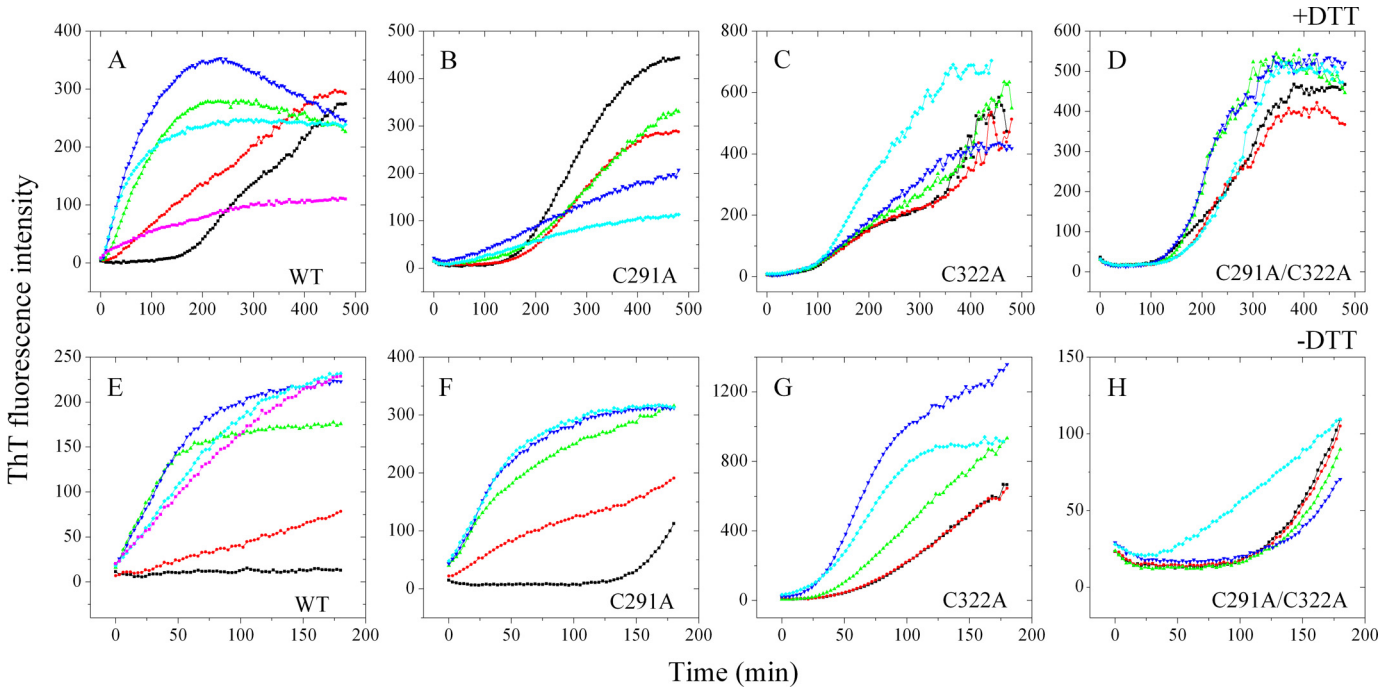

FIGURE 4. **Cys-291 and Cys-322 are key residues in the interaction of Zn^{2+} with $Tau_{244-372}$.** The *top panels* show the ThT binding assays of 20 μM wild-type (*WT*) $Tau_{244-372}$ (*A*), 20 μM single mutants C291A (*B*), and C322A (*C*) or double mutant C291A/C322A (*D*) incubated with 0–80 μM Zn^{2+} (*black*, 0 μM; *red*, 4 μM; *green*, 10 μM; *blue*, 20 μM; *cyan*, 40 μM; and *magenta*, 80 μM) in the presence of 1 mM DTT. The *bottom panels* show the ThT binding assays of 20 μM WT $Tau_{244-372}$ (*E*), 20 μM single mutants C291A (*F*), and C322A (*G*) or double mutant C291A/C322A (*H*) incubated with 0–80 μM Zn^{2+} (*black*, 0 μM; *red*, 4 μM; *green*, 10 μM; *blue*, 20 μM; *cyan*, 40 μM; and *magenta*, 80 μM) in the absence of DTT. The assays were carried out at 37 °C, and the samples were incubated in 50 mM Tris-HCl buffer (pH 7.5) containing 100 mM NaCl, 5 μM heparin and 50 μM ThT.

Effect of Zn^{2+} on Tau Aggregation under Reducing or Oxidative Conditions—Neuronal cells normally have a reducing environment maintained by an excess of glutathione (1, 5, 37). To mimic the reducing environment present in normal neuronal cells and block the formation of an intramolecular disulfide bond, DTT, a strong reducing agent, was used in this study. We carried out ThT binding assays in the presence and absence of DTT to compare the effect of Zn^{2+} on Tau aggregation under reducing conditions with that in oxidizing conditions. Additionally, 100 mM NaCl was added into the polymerization mixture to mimic the physiological salinity. It has been reported that Tau aggregation is highly sensitive to elevated ionic strength (38). As shown in Fig. 4*A*, in the presence of DTT and 100 mM NaCl, the results were quite similar to those obtained in the presence of DTT but without salt (Fig. 1), except that the lag time of Tau fibrillization was much longer than that in the absence of salt as expected. When wild-type $Tau_{244-372}$ was incubated with low micromolar concentrations of Zn^{2+}, the kinetic curves of Tau fibrillization grew much faster and reached a plateau around 3 h, compared with >8 h in the absence of Zn^{2+}, once again indicating that low micromolar concentrations of Zn^{2+} dramatically accelerated fibril formation of wild-type $Tau_{244-372}$ under physiological reducing conditions.

While in the absence of DTT (Fig. 4*E*), the kinetic curve of Tau fibrillization showed no detectable increase within 3 h in the absence of Zn^{2+}. But when $Tau_{244-372}$ was incubated with different concentrations of Zn^{2+}, the kinetic curves showed instant increases in oxidizing conditions even at higher molar ratios of Zn^{2+} to Tau. It is quite different from those obtained in reducing conditions, which showed smaller exponential growth and much lower final ThT intensities at higher molar ratios of Zn^{2+} to Tau (Fig. 4*A*). This comparison suggests that higher concentrations of Zn^{2+} induced Tau to form granular aggregates only under reducing conditions.

Cys-291 and Cys-322 Are Key Residues in the Interaction of Zn^{2+} with Tau—There are two cysteine residues, Cys-291 and Cys-322, in full-length human Tau protein (441 amino acids). They are located in repeats 2 and 3 of the four-repeat microtubule binding domain (37, 39). Little is known about the role of such cysteine residues in Tau assembly, because their substitution with other amino acids has no effect on Tau filament morphology (40). In this study, $Tau_{244-372}$ mutants containing single and double cysteine mutations were designed, and ThT binding assays using such mutants were performed to provide information about the binding sites of zinc in Tau protein and the role of Cys-291 and Cys-322 in Tau assembly. Table 1 summarizes the kinetic parameters obtained for fibril formation of wild-type $Tau_{244-372}$ and its cysteine mutants in the presence of low micromolar concentrations of Zn^{2+} under reducing conditions. Unlike wild-type $Tau_{244-372}$, 4–10 μM Zn^{2+} had no obvious effects on fibrillization kinetics of single mutants C291A and C322A and double mutant C291A/C322A in reducing conditions (Fig. 4, *B–D*, and Table 1), indicating that low micromolar zinc accelerated the fibrillization of human Tau protein via bridging Cys-291 and Cys-322. But higher concentrations of Zn^{2+} did not have uniform effects on fibrillization kinetics of $Tau_{244-372}$ mutants under reducing conditions: an inhibitory effect on C291A (Fig. 4*B*), an enhancing effect on C322A (Fig. 4*C*), and no obvious enhancing effect on C291A/

C322A (Fig. 4*D*). The above results suggest that, under physiological reducing conditions, Cys-291 and Cys-322 are key residues in the interaction of Zn^{2+} with Tau protein.

While under oxidative conditions, the addition of different concentrations of Zn^{2+} showed remarkable enhancing effects on fibrillization kinetics of wild-type $Tau_{244-372}$ and single mutants C291A and C322A but had no obvious effect on double mutant C291A/C322A (Fig. 4, *E–H*), suggesting that, in oxidizing conditions, Cys-291 and Cys-322 are also key residues in the interaction of Zn^{2+} with Tau protein. The presence of Cys-291 and Cys-322 gives rise to a tendency to form an intramolecular disulfide bond and thus generate compact Tau monomers under oxidative conditions (41, 42). Clearly, the formation of such intramolecular disulfide bonds was unfavorable to fibril formation of $Tau_{244-372}$, and zinc accelerated filament formation of Tau protein by inhibiting the formation of intramolecular disulfide bonds and enhancing intermolecular ones in oxidative conditions (Fig. 4, *E–G*).

TABLE 1

Kinetic parameters of $Tau_{244-372}$ fibrillization in the presence of low micromolar concentrations of Zn^{2+} as determined by ThT binding assays at 37 °C

Kinetic parameters, k, t_m, and the lag time, were determined by fitting ThT fluorescence intensity *versus* time to Equation 1. The buffer used was 50 mM Tris-HCl buffer (pH 7.5) containing 1 mM DTT, 100 mM NaCl, 5 μM heparin, and 50 μM ThT. Errors shown are ± S.E.

$Tau_{244-372}$	Zn^{2+}	k	t_m	Lag time
	μM	10^{-3} min^{-1}	min	min
WT[a]	0	37.3 ± 4.0	176 ± 4	122 ± 10
	4	35.1 ± 9.5	38.2 ± 11	0[b]
	10	17.6 ± 0.6	48.0 ± 3.7	0[b]
C291A	0	22.2 ± 0.4	253 ± 2	163 ± 4
	4	21.1 ± 0.4	273 ± 3	178 ± 5
	10	15.6 ± 0.3	257 ± 7	129 ± 9
C322A	0	ND[c]	ND	100[b]
	4	ND	ND	100[b]
	10	ND	ND	70[b]
DM[d]	0	16.0 ± 0.5	304 ± 8	179 ± 12
	4	17.8 ± 0.9	283 ± 9	171 ± 15
	10	26.3 ± 1.3	227 ± 3	151 ± 7

[a] WT, wild-type $Tau_{244-372}$.
[b] Observed from the ThT fluorescence curves directly.
[c] ND, not determined because the ThT fluorescence data in the present conditions could not be fitted to such a sigmoidal equation.
[d] DM, double mutant C291A/C322A of $Tau_{244-372}$.

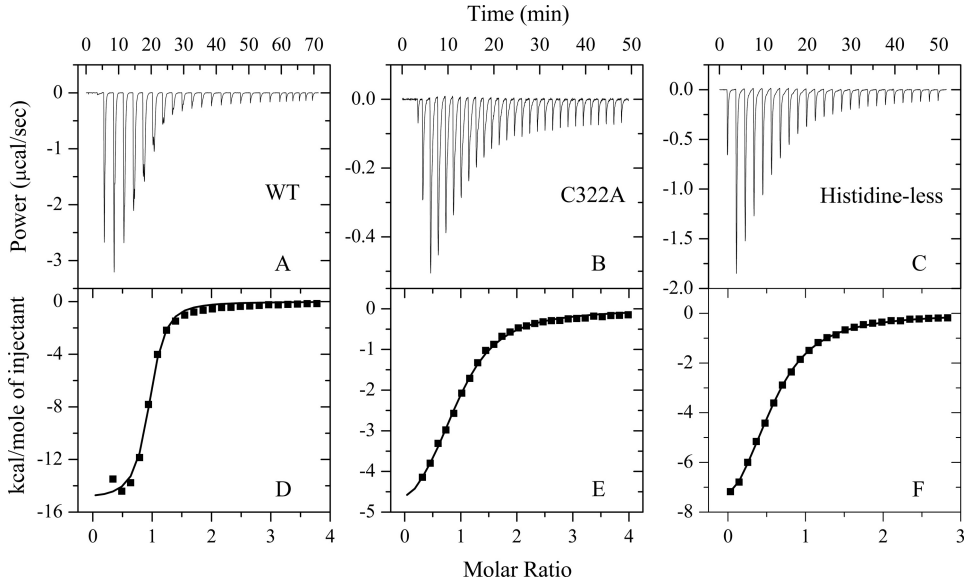

FIGURE 5. **ITC profiles for the binding of Zn^{2+} to wild-type $Tau_{244-372}$ and its mutants at 25. 0 °C.** The *top panels* represent the raw data for sequential 1-μl injections of Zn^{2+} (6.0, 2.8, and 4.5 mM for *A*, *B*, and *C*, respectively) into 200 μM wild-type (WT) $Tau_{244-372}$ (*A*), 100 μM single mutant C322A (*B*), and 200 μM histidine-less mutant H268A/H299A/H329A/H330A/H362A in 50 mM Tris-HCl buffer (pH 7.5) (*C*), respectively. The *bottom panels* (*D*, *E*, and *F*) show the plots of the heat evolved (kilocalories) per mole of Zn^{2+} added, corrected for the heat of Zn^{2+} dilution, against the molar ratio of Zn^{2+} to $Tau_{244-372}$. The data (*solid squares*) were best fitted to a single set of identical sites model, and the *solid lines* represent the best fit.

Thermodynamics of the Binding of Zn^{2+} to Tau—ITC provides a direct route to the complete thermodynamic characterization of non-covalent, equilibrium interactions (32, 43), and DTT concentrations as low as 1 mM can cause severe baseline artifacts due to background oxidation during the titration. Therefore ITC was used to measure the binding affinity of Zn^{2+} to Tau monomer in the absence of DTT. ITC profiles for the binding of Zn^{2+} to wild-type $Tau_{244-372}$, single cysteine mutant C322A, and the histidine-less mutant at 25.0 °C are shown in Fig. 5. The *top panels* in Fig. 5 representatively show raw ITC curves resulting from the injections of Zn^{2+} into a solution of wild-type $Tau_{244-372}$ (Fig. 5*A*), C322A (Fig. 5*B*), and histidine-less mutant (Fig. 5*C*). The titration curves show that zinc binding to wild-type $Tau_{244-372}$ and its mutants is exothermic, resulting in negative peaks in the plots of power *versus* time. The *bottom panels* in Fig. 5 show the plot of the heat evolved per mole of Zn^{2+} added, corrected for the heat of Zn^{2+} dilution, against the molar ratio of Zn^{2+} to wild-type $Tau_{244-372}$ (Fig. 5*D*), C322A (Fig. 5*E*), and histidine-less mutant (Fig. 5*F*). The calorimetric data were best fit to a model assuming a single set of identical sites. The thermodynamic parameters for the binding of Zn^{2+} to $Tau_{244-372}$ are summarized in Table 2. As shown in Table 2, one Zn^{2+} bound to one wild-type $Tau_{244-372}$ molecule with a dissociation constant of 3.82 μM. The binding affinities of Zn^{2+} to single cysteine mutants C291A and C322A were significantly lower than that of wild-type $Tau_{244-372}$, with a dissociation constant of 9.71 and 20.2 μM, respectively. No binding reaction for Zn^{2+} with double cysteine mutant C291A/C322A was detected by ITC (Table 2), demonstrating that Cys-291 and Cys-322 are key residues in the interaction of Zn^{2+} with Tau protein. Because it is known that zinc prefers tetrahedral coordination (44), we wanted to know what the remaining zinc ligands were. As shown in Table 2, the binding affinities of Zn^{2+} to single histidine mutants H330A and H362A and histidine-less mutant were remarkably lower than that of wild-type $Tau_{244-372}$, suggesting that His-330 and His-362 are probably the remaining zinc ligands.

DISCUSSION

Zn^{2+} Modulates Tau Aggregation via Bridging Cys-291 and Cys-322—During the past decade, several models describing the fibril formation of human Tau protein have

TABLE 2

Thermodynamic parameters for the binding of Zn^{2+} to $Tau_{244-372}$ as determined by ITC at 25.0 °C

Thermodynamic parameters, K_d, $\Delta_b H^0_m$, and n, were determined using a single set of identical sites model. The standard molar binding free energy ($\Delta_b G^0_m$) and the standard molar binding entropy ($\Delta_b S^0_m$) for the binding reaction were calculated using Equations 2 and 3, respectively. The buffer used was 50 mM Tris-HCl buffer (pH 7.5). Errors shown are ± S.E.

$Tau_{244-372}$	K_d	n	$\Delta_b H^0_m$	$\Delta_b G^0_m$	$\Delta_b S^0_m$
	μM		*kcal mol*$^{-1}$	*kcal mol*$^{-1}$	*cal mol*$^{-1}$ *K*$^{-1}$
WT[a]	3.82 ± 0.65	0.905 ± 0.012	−15.0 ± 0.3	−7.39 ± 0.10	−25.6 ± 1.3
C291A	9.71 ± 0.62	0.443 ± 0.009	−10.1 ± 0.27	−6.83 ± 0.04	−11.1 ± 1.1
C322A	20.2 ± 1.2	0.922 ± 0.017	−5.62 ± 0.14	−6.40 ± 0.04	2.62 ± 0.59
DM[b]	NB[c]	—	—	—	—
H330A	8.77 ± 1.08	0.584 ± 0.012	−13.7 ± 0.46	−6.90 ± 0.07	−22.7 ± 1.8
H362A	5.92 ± 2.44	0.622 ± 0.038	−3.80 ± 0.27	−7.13 ± 0.24	11.2 ± 1.7
Histidine-less[d]	38.3 ± 0.8	0.556 ± 0.004	−9.75 ± 0.09	−6.02 ± 0.01	−12.5 ± 0.3

[a] WT, wild-type $Tau_{244-372}$.
[b] DM, double mutant C291A/C322A of $Tau_{244-372}$.
[c] NB, no binding observed in the present conditions.
[d] Histidine-less, histidine-less mutant H268A/H299A/H329A/H330A/H362A.

been proposed to characterize the mechanism and key factors in this process (1, 35, 37, 38, 42, 45–47). A typical Tau filament pathway starts with the formation of assembly-competent intermediates, which then form fibrils following classic nucleation-dependent kinetics characterized by a lag period, followed by a period of exponential growth and an asymptotic approach to equilibrium (35, 45). The "driving force" for filament formation by Tau protein involves both the formation of an intermolecular disulfide bond (35) and non-covalent intermolecular interactions such as hydrogen bonds between all pairs of adjacent β-strands (48), electrostatic interactions between the negatively charged heparin and the basic lysine residues of Tau (49), and hydrophobic interactions between Tau molecules and between Tau and heparin (50). Any structural change to enhance the driving force should promote the fibril formation of human Tau molecules. In this study, we demonstrated that low micromolar zinc dramatically accelerated fibril formation of wild-type $Tau_{244-372}$ but had no obvious effects on fibrillization kinetics of single mutants C291A and C322A and double mutant C291A/C322A and thus suggested that low micromolar zinc accelerated the fibrillization of human Tau protein via bridging Cys-291 and Cys-322 under physiological reducing conditions. In other words, the enhancing effect of low micromolar concentrations of Zn^{2+} depended on intermolecular disulfide bridges formed by Cys-291 and Cys-322. In contrast, higher concentrations of Zn^{2+} inhibited Tau fibrillization and induced wild-type $Tau_{244-372}$ to form granular aggregates but still had no noticeable effect on the double mutant in reductive conditions. The binding of Zn^{2+} to Tau monomer is an exothermic reaction, which is favorable to the non-covalent intermolecular interactions as described above. Therefore, under reducing conditions, low micromolar zinc enhanced both the formation of intermolecular disulfide bridges between Cys-291 and Cys-322 and these non-covalent intermolecular interactions to promote Tau fibrillization. But higher concentrations of Zn^{2+} strongly inhibited the formation of intermolecular disulfide bridges between Cys-291 and Cys-322 and thus inhibited Tau fibrillization. All the evidence above strongly supports our finding that Zn^{2+} modulates Tau aggregation via bridging Cys-291 and Cys-322 in reducing conditions.

Under oxidative conditions (air oxidation), however, a prerequisite for nucleation is the dimerization of Tau, because Tau dimers act as effective building blocks (35), and dimerization and nucleation are the rate-limiting steps for PHF formation (47). Furthermore, a dimeric Tau with an intermolecular disulfide bond is presumably acting as a seed for initiation of Tau polymerization (39), and the presence of PHF6 hexapeptide and one cysteine residue is a minimum requirement for efficient assembly of cysteine-dependent Tau dimer (40). The present study demonstrated that the effect of zinc on Tau assembly can be affected by the oxidative/reductive state of experimental conditions. In oxidizing conditions, the addition of Zn^{2+} even at high concentrations showed remarkable enhancing effects on fibrillization kinetics of wild-type $Tau_{244-372}$ and single mutants C291A and C322A but had no obvious effect on the double mutant. This finding suggests that Zn^{2+} enhances Tau fibrillization by inhibiting the formation of intramolecular disulfide bonds and promoting the formation of the dimeric Tau with an intermolecular disulfide bond through either Cys-291 or Cys-322 under oxidative conditions.

Characterization of the Zinc Binding Sites of Tau—As an essential element, Zn^{2+} has been found to play a catalytic or structural role in many proteins (13, 51). In catalytic zinc sites, Zn^{2+} generally forms complexes with water and any three nitrogen, oxygen, and sulfur donors with His being the predominant amino acid chosen. In structural zinc sites, however, Zn^{2+} is found tetrahedrally coordinated to amino acid residues and bound preferentially to Cys (44). In this case, Zn^{2+} bound to Tau protein via tetrahedral coordination to Cys-291 and Cys-322 as well as two histidines, which are assumed to be His-330 and His-362, and thus modulated the assembly kinetics and morphology of aggregates of human Tau protein associated with Alzheimer disease. This finding suggests that Zn^{2+} should play a structural role but not a catalytic role in the aggregation of Tau protein.

Zinc Plays a Significant Role in the Development of Tau Pathology—A hallmark of a group of neurodegenerative diseases such as Alzheimer disease is the formation of NFTs, which are principally composed of bundles of filaments formed by microtubule-associated protein Tau (1–3, 52–54). There is considerable evidence showing that zinc, as an essential element that is highly concentrated in brain, is linked to the development or progression of these diseases (13). Brain zinc is generally divided into two types, protein-bound and loosely bound, the latter also being termed mobile zinc (55). Alterations in zinc

metabolism and homeostasis have been reported in such neurodegenerative diseases (10–12). Therefore, further elucidation of the pathological actions of Zn^{2+} in the brain should result in new therapeutic approaches to these neurodegenerative diseases.

Zn^{2+} has been reported to bind to several proteins/peptides associated with neurodegenerative diseases, including human amyloid β peptides (21, 56, 57), human prion protein (58, 59) and human α-synuclein (23). Zinc binding has been shown to modulate the aggregation behavior of these amyloidogenic proteins. For instance, zinc binding promotes fibril formation of human amyloid β peptides associated with Alzheimer disease (21, 22). Zn^{2+} has been used to modulate the assembly kinetics and morphology of congeners of amyloid β peptide (60), and low micromolar zinc significantly reduces amyloid β toxicity (61). Human α-synuclein, a protein associated with Parkinson disease, is intrinsically unfolded (62) and Zn^{2+} binding triggers the fibrillization of methionine oxidized α-synuclein (23). The abnormal form of prion protein is believed to be responsible for transmissible spongiform encephalopathy (63, 64), and copper and zinc binding modulates the aggregation and neurotoxic properties of the human prion peptide prion protein 106–126 (58). Our work continues the long story of the possible role of metal ions such as zinc in forming fibrils. We demonstrated for the first time that one Zn^{2+} binds to one Tau monomer via tetrahedral coordination to the two cysteines of human Tau protein, Cys-291 and Cys-322, and two histidines, with a moderate affinity similar to that between Zn^{2+} and amyloid β (21, 56, 57). We also found that the Tau fibrils formed in the presence of low micromolar Zn^{2+} showed significant dose-dependent cytotoxicity to SH-SY5Y neuroblastoma cells when SH-SY5Y cells were treated with such fibrils for 24 h (data not shown). Taken together, these results indicate that Zn^{2+} directly binds to Tau protein via tetrahedral coordination to Cys-291 and Cys-322 as well as two histidines, and thereby modulates Tau aggregation in physiological reducing conditions. Thus, it seems reasonable to speculate that Alzheimer disease, Parkinson disease, and transmissible spongiform encephalopathy share common mechanisms of metal ion (including zinc ion) regulation of amyloidogenic protein aggregation, which might lead to a common (65), or at least one or more overlapping, pathogenic mechanisms.

In addition to this direct interaction between Zn^{2+} and human Tau protein we observed, it is also known that many of the kinases that phosphorylate Tau (ultimately resulting in hyperphosphorylation and dissociation from the microtubules), such as the extracellular signal-regulated kinase, can be induced by Zn^{2+} (66, 67). Zinc has a bimodal effect on Tau phosphorylation depending on the zinc concentration and induces glycogen synthase kinase-3β activation and Tau release from microtubules (68). The interaction of Tau protein with its partner S100β is promoted by zinc and inhibited by hyperphosphorylation in Alzheimer disease (69). All the results above suggest that zinc plays a significant role in the onset and development of Tau pathology associated to neurodegenerative diseases by increasing the formation of neurotoxic fibrils of Tau protein.

In conclusion we have shown that: (i) fibril formation of Tau protein from natively unstructured monomers proceeds slowly in the absence of Zn^{2+}; (ii) low micromolar concentrations of Zn^{2+} dramatically accelerate fibril formation of Tau in both reducing conditions and oxidative conditions; (iii) higher concentrations of Zn^{2+} induce Tau to form granular aggregates only under reducing conditions, and these non-fibrillar aggregates assemble into mature Tau filaments when Zn^{2+} has been chelated by EDTA; (iv) one Zn^{2+} binds to one Tau monomer via tetrahedral coordination to Cys-291 and Cys-322 as well as two histidines, with moderate, micromolar affinity, in oxidizing conditions. Our data demonstrate that low micromolar zinc accelerates the fibrillization of human Tau protein via bridging Cys-291 and Cys-322 in physiological reducing conditions, providing clues to understanding the relationship between zinc dyshomeostasis and the etiology of neurodegenerative diseases. The enhancing effect of zinc on Tau fibrillization occurred at concentrations 10- to 30-fold lower than the 100–300 μM zinc concentration present in synaptic vesicles of the brain, implicating an important role for zinc in Tau aggregation and toxicity in the Alzheimer disease brain.

Acknowledgments—We sincerely thank Dr. Michel Goedert (Laboratory of Molecular Biology, Medical Research Council, Cambridge, UK) for kindly providing the plasmid for human Tau40 and Dr. Frank Shewmaker (NIDDK, National Institutes of Health, Bethesda) for his critical reading of the manuscript. We thank Prof. Guang-Fu Yang (College of Chemistry, Central China Normal University, Wuhan, China), Dr. Sheng Xu (College of Physical Science and Technology, Wuhan University, Wuhan, China), and Dr. Li Li (College of Life Sciences, Wuhan University, Wuhan, China) for their technical assistances on iTC_{200}, AFM, and TEM, respectively.

REFERENCES

1. Kuret, J., Chirita, C. N., Congdon, E. E., Kannanayakal, T., Li, G., Necula, M., Yin, H., and Zhong, Q. (2005) *Biochim. Biophys. Acta* **1739,** 167–178
2. Skovronsky, D. M., Lee, V. M., and Trojanowski, J. Q. (2006) *Annu. Rev. Pathol.* **1,** 151–170
3. Braak, H., and Braak, E. (1997) *Neurobiol. Aging* **18,** 351–357
4. Mandelkow, E., Song, Y. H., Schweers, O., Marx, A., and Mandelkow, E. M. (1995) *Neurobiol. Aging* **16,** 347–354
5. Rosenberg, K. J., Ross, J. L., Feinstein, H. E., Feinstein, S. C., and Israelachvili, J. (2008) *Proc. Natl. Acad. Sci. U.S.A.* **105,** 7445–7450
6. Ballatore, C., Lee, V. M., and Trojanowski, J. Q. (2007) *Nat. Rev. Neurosci.* **8,** 663–672
7. Mandelkow, E., von Bergen, M., Biernat, J., and Mandelkow, E. M. (2007) *Brain Pathol.* **17,** 83–90
8. Wille, H., Drewes, G., Biernat, J., Mandelkow, E. M., and Mandelkow, E. (1992) *J. Cell Biol.* **118,** 573–584
9. Wischik, C. M., Novak, M., Thøgersen, H. C., Edwards, P. C., Runswick, M. J., Jakes, R., Walker, J. E., Milstein, C., Roth, M., and Klug, A. (1988) *Proc. Natl. Acad. Sci. U.S.A.* **85,** 4506–4510
10. Bush, A. I. (2000) *Curr. Opin. Chem. Biol.* **4,** 184–191
11. Barnham, K. J., and Bush, A. I. (2008) *Curr. Opin. Chem. Biol.* **12,** 222–228
12. Cuajungco, M. P., and Lees, G. J. (1997) *Brain Res. Rev.* **23,** 219–236
13. Weiss, J. H., Sensi, S. L., and Koh, J. Y. (2000) *Trends Pharmacol. Sci.* **21,** 395–401
14. Koh, J. Y. (2001) *Mol. Neurobiol.* **24,** 99–106
15. Frederickson, C. J., Koh, J. Y., and Bush, A. I. (2005) *Nat. Rev. Neurosci.* **6,** 449–462
16. Thompson, C. M., Markesbery, W. R., Ehmann, W. D., Mao, Y. X., and Vance, D. E. (1988) *Neurotoxicology* **9,** 1–7

17. Assaf, S. Y., and Chung, S. H. (1984) *Nature* **308,** 734–736
18. Hutchinson, R. W., Cox, A. G., McLeod, C. W., Marshall, P. S., Harper, A., Dawson, E. L., and Howlett, D. R. (2005) *Anal. Biochem.* **346,** 225–233
19. Adlard, P. A., and Bush, A. I. (2006) *J. Alzheimers Dis.* **10,** 145–163
20. Lovell, M. A., Robertson, J. D., Teesdale, W. J., Campbell, J. L., and Markesbery, W. R. (1998) *J. Neurol. Sci.* **158,** 47–52
21. Bush, A. I., Pettingell, W. H., Multhaup, G., d Paradis, M., Vonsattel, J. P., Gusella, J. F., Beyreuther, K., Masters, C. L., and Tanzi, R. E. (1994) *Science* **265,** 1464–1467
22. Huang, X., Atwood, C. S., Moir, R. D., Hartshorn, M. A., Vonsattel, J. P., Tanzi, R. E., and Bush, A. I. (1997) *J. Biol. Chem.* **272,** 26464–26470
23. Yamin, G., Glaser, C. B., Uversky, V. N., and Fink, A. L. (2003) *J. Biol. Chem.* **278,** 27630–27635
24. Blumenthal, J., and Ginzburg, I. (2008) *J. Cell Sci.* **121,** 3253–3260
25. Yang, L. S., and Ksiezak-Reding, H. (1999) *J. Neurosci. Res.* **55,** 36–43
26. Shin, R. W., Lee, V. M., and Trojanowski, J. Q. (1994) *J. Neurosci.* **14,** 7221–7233
27. Soragni, A., Zambelli, B., Mukrasch, M. D., Biernat, J., Jeganathan, S., Griesinger, C., Ciurli, S., Mandelkow, E., and Zweckstetter, M. (2008) *Biochemistry* **47,** 10841–10851
28. Sayre, L. M., Perry, G., Harris, P. L., Liu, Y., Schubert, K. A., and Smith, M. A. (2000) *J. Neurochem.* **74,** 270–279
29. Barghorn, S., Biernat, J., and Mandelkow, E. (2005) *Methods Mol. Biol.* **299,** 35–51
30. Chattopadhyay, M., Durazo, A., Sohn, S. H., Strong, C. D., Gralla, E. B., Whitelegge, J. P., and Valentine, J. S. (2008) *Proc. Natl. Acad. Sci. U.S.A.* **105,** 18663–18668
31. Aoyagi, H., Hasegawa, M., and Tamaoka, A. (2007) *J. Biol. Chem.* **282,** 20309–20318
32. Xu, H., Liang, Y., Zhang, P., Du, F., Zhou, B. R., Wu, J., Liu, J. H., Liu, Z. G., and Ji, L. N. (2005) *J. Biol. Inorg. Chem.* **10,** 529–538
33. Naiki, H., Higuchi, K., Hosokawa, M., and Takeda, T. (1989) *Anal. Biochem.* **177,** 244–249
34. Yang, F., Jr., Zhang, M., Zhou, B. R., Chen, J., and Liang, Y. (2006) *J. Mol. Biol.* **362,** 821–834
35. Friedhoff, P., von Bergen, M., Mandelkow, E. M., Davies, P., and Mandelkow, E. (1998) *Proc. Natl. Acad. Sci. U.S.A.* **95,** 15712–15717
36. Maeda, S., Sahara, N., Saito, Y., Murayama, M., Yoshiike, Y., Kim, H., Miyasaka, T., Murayama, S., Ikai, A., and Takashima, A. (2007) *Biochemistry* **46,** 3856–3861
37. Friedhoff, P., von Bergen, M., Mandelkow, E. M., and Mandelkow, E. (2000) *Biochim. Biophys. Acta* **1502,** 122–132
38. Friedhoff, P., Schneider, A., Mandelkow, E. M., and Mandelkow, E. (1998) *Biochemistry* **37,** 10223–10230
39. Bhattacharya, K., Rank, K. B., Evans, D. B., and Sharma, S. K. (2001) *Biochem. Biophys. Res. Commun.* **285,** 20–26
40. Sahara, N., Maeda, S., Murayama, M., Suzuki, T., Dohmae, N., Yen, S. H., and Takashima, A. (2007) *Eur. J. Neurosci.* **25,** 3020–3029
41. Schweers, O., Mandelkow, E. M., Biernat, J., and Mandelkow, E. (1995) *Proc. Natl. Acad. Sci. U.S.A.* **92,** 8463–8467
42. Barghorn, S., and Mandelkow, E. (2002) *Biochemistry* **41,** 14885–14896
43. Liang, Y., Du, F., Sanglier, S., Zhou, B. R., Xia, Y., Van Dorsselaer, A., Maechling, C., Kilhoffer, M. C., and Haiech, J. (2003) *J. Biol. Chem.* **278,** 30098–30105
44. Lee, Y. M., and Lim, C. (2008) *J. Mol. Biol.* **379,** 545–553
45. Chirita, C. N., and Kuret, J. (2004) *Biochemistry* **43,** 1704–1714
46. von Bergen, M., Barghorn, S., Biernat, J., Mandelkow, E. M., and Mandelkow, E. (2005) *Biochim. Biophys. Acta* **1739,** 158–166
47. Congdon, E. E., Kim, S., Bonchak, J., Songrug, T., Matzavinos, A., and Kuret, J. (2008) *J. Biol. Chem.* **283,** 13806–13816
48. Li, D.W., Mohanty, S., Irbäck, A., and Huo, S. (2008) *PLoS Comput. Biol.* **4,** e1000238
49. Sibille, N., Sillen, A., Leroy, A., Wieruszeski, J. M., Mulloy, B., Landrieu, I., and Lippens, G. (2006) *Biochemistry* **45,** 12560–12572
50. Jeganathan, S., von Bergen, M., Mandelkow, E. M., and Mandelkow, E. (2008) *Biochemistry* **47,** 10526–10539
51. Vallee, B. L., and Falchuk, K. H. (1993) *Physiol. Rev.* **73,** 79–118
52. Goedert, M. (1993) *Trends Neurosci.* **16,** 460–465
53. Mandelkow, E. M., and Mandelkow, E. (1993) *Trends. Biochem. Sci.* **18,** 480–483
54. Goedert, M., Jakes, R., Spillantini, M. G., Hasegawa, M., Smith, M. J., and Crowther, R. A. (1996) *Nature* **383,** 550–553
55. Nolan, E. M., and Lippard, S. J. (2009) *Acc. Chem. Res.* **42,** 193–203
56. Talmard, C., Bouzan, A., and Faller, P. (2007) *Biochemistry* **46,** 13658–13666
57. Tõugu, V., Karafin, A., and Palumaa, P. (2008) *J. Neurochem.* **104,** 1249–1259
58. Jobling, M. F., Huang, X., Stewart, L. R., Barnham, K. J., Curtain, C., Volitakis, I., Perugini, M., White, A. R., Cherny, R. A., Masters, C. L., Barrow, C. J., Collins, S. J., Bush, A. I., and Cappai, R. (2001) *Biochemistry* **40,** 8073–8084
59. Gaggelli, E., Bernardi, F., Molteni, E., Pogni, R., Valensin, D., Valensin, G., Remelli, M., Luczkowski, M., and Kozlowski, H. (2005) *J. Am. Chem. Soc.* **127,** 996–1006
60. Dong, J., Shokes, J. E., Scott, R. A., and Lynn, D. G. (2006) *J. Am. Chem. Soc.* **128,** 3540–3542
61. Garai, K., Sahoo, B., Kaushalya, S. K., Desai, R., and Maiti, S. (2007) *Biochemistry* **46,** 10655–10663
62. Fink, A. L. (2006) *Acc. Chem. Res.* **39,** 628–634
63. Prusiner, S. B. (1998) *Proc. Natl. Acad. Sci. U.S.A.* **95,** 13363–13383
64. Soto, C., Estrada, L., and Castilla, J. (2006) *Trends Biochem. Sci.* **31,** 150–155
65. Soto, C. (2003) *Nat. Rev. Neurosci.* **4,** 49–60
66. An, W. L., Bjorkdahl, C., Liu, R., Cowburn, R. F., Winblad, B., and Pei, J. J. (2005) *J. Neurochem.* **92,** 1104–1115
67. Harris, F. M., Brecht, W. J., Xu, Q., Mahley, R. W., and Huang, Y. (2004) *J. Biol. Chem.* **279,** 44795–44801
68. Boom, A., Authelet, M., Dedecker, R., Frédérick, C., Van Heurck, R., Daubie, V., Leroy, K., Pochet, R., and Brion, J. P. (2009) *Biochim. Biophys. Acta* **1793,** 1058–1067
69. Yu, W. H., and Fraser, P. E. (2001) *J. Neurosci.* **21,** 2240–2246